

# In silico Analysis of Two Novel Variants in the Pyruvate Carboxylase (PC) Gene Associated with the Severe Form of PC Deficiency

Fereshteh Maryami<sup>1</sup>, Elham Rismani<sup>1</sup>, Elham Davoudi-Dehaghani<sup>1</sup>, Nasrin Khalesi<sup>2\*</sup>, Saeed Talebi<sup>3</sup>, Reza Mahdian<sup>1</sup>, Sirous Zeinali<sup>1,4\*</sup>

<sup>1</sup>Department of Molecular Medicine, Biotechnology Research Center, Pasteur Institute of Iran, Pasteur St., Tehran, Iran; <sup>2</sup>Department of Pediatrics and Neonatal Intensive Care Unit, Ali-Asghar Children's Hospital, Iran University of Medical Sciences, Tehran, Iran; <sup>3</sup>Department of Medical Genetics and Molecular Biology, Faculty of Medicine, Iran University of Medical Sciences (IUMS), Tehran, Iran; <sup>4</sup>Kawsar Human Genetics Research Center, Tehran, Iran

## OPEN ACCESS

**Received:** 8 April 2023  
**Accepted:** 17 June 2023  
**Published online:** 19 June 2023

## ABSTRACT

**Background:** Inborn errors of metabolism are a common cause of neonatal death. This study evaluated the acute early-onset metabolic derangement and death in two unrelated neonates.

**Methods:** WES, Sanger sequencing, homology modeling, and in silico bioinformatics analysis were employed to assess the effects of variants on protein structure and function.

**Results:** WES revealed a novel homozygous variant, p.G303Afs\*40 and p.R156P, in the PC gene of each neonate, which both were confirmed by Sanger sequencing. Based on the ACMG guidelines, the p.G303Afs\*40 was likely pathogenic, and the p.R156P was a VUS. Nevertheless, a known variant at position 156, the p.R156Q, was also a VUS. Protein secondary structure prediction showed changes in p.R156P and p.R156Q variants compared to the wild-type protein. However, p.G303Afs\*40 depicted significant changes at C-terminal. Furthermore, comparing the interaction of wild-type and variant proteins with the ATP ligand during simulations, revealed a decreased affinity to the ATP in all the variants. Moreover, analysis of SNP impacts on PC protein using Polyphen-2, SNAP2, FATHMM, and SNPs&GO servers predicted both R156P and R156Q as damaging variants. Likewise, free energy calculations demonstrated the destabilizing effect of both variants on PC.

**Conclusion:** This study confirmed the pathogenicity of both variants and suggested them as a cause of type B PCD. The results of this study would provide the family with prenatal diagnosis and expand the variant spectrum in the PC gene, which is beneficial for geneticists and endocrinologists.

**DOI:** 10.61186/ibj.27.5.307

**Keywords:** Pyruvate carboxylase, Pyruvate carboxylase deficiency disease, Metabolic diseases, Exome sequencing

## Citation:

Maryami F, Rismani E, Davoudi-Dehaghani E, Khalesi N, Talebi S, Mahdian R, Zeinali S. In silico Analysis of Two Novel Variants in the Pyruvate Carboxylase (PC) Gene Associated with the Severe Form of PC Deficiency. *Iranian biomedical journal* 2023; 27(5): 307-319.

## Corresponding Authors:

Nasrin Khalesi

Department of Pediatrics and neonatal intensive care unit, Ali-Asghar Children's Hospital, Shahid Vahid Dastgerdi Street, Modarres Highway, Tehran, Iran; Mobile: (+98-912) 4000379; E-mail: nasrinkhalesi@yahoo.com

Sirous Zeinali

Department of Molecular Medicine, Biotechnology Research Center, Pasteur Institute of Iran, Pasteur St., Tehran, Iran; Medical Genetics Lab, Kawsar Human Genetics Research Center, No. 41 Majlesi St., ValiAsr St., Tehran 1595645513, Iran; Tel.: (+98-21) 88939140; Mobile: (+98-912) 1372040; Fax: (+98-21) 88930868; E-mail: zeinali@gmail.com

Both corresponding authors contributed equally to this work.

## List of Abbreviations:

**2D:** two-dimensional; **3D:** Three-dimensional; **ACMG:** American College of Medical Genetics and Genomics; **BC:** biotin carboxylation domain of PC; **BCCP:** biotin carboxyl carrier domain of PC; **CT:** transcarboxylation domain of PC; **FATHMM:** Functional Analysis Through Hidden Markov Models; **GMQE:** Global Model Quality Estimate; **LFT:** Liver function test; **NICU:** Neonatal Intensive Care Unit; **PC:** pyruvate carboxylase; **PCD:** Pyruvate carboxylase deficiency; **PolyPhen-2:** polymorphism Phenotyping v2; **PSIPRED:** PSI-blast based secondary structure PREDiction; **RMSF:** root-mean-square fluctuation; **SNAP2:** screening for non-acceptable polymorphisms; **SNP:** single nucleotide polymorphism; **SNV:** single nucleotide variant; **VUS:** variant of uncertain significance; **WES:** whole-exome sequencing

## INTRODUCTION

The *PC* gene (NG\_008319.1), of 109,964 bp in length, is located at chromosome 11q13.2 and has three tissue-specific mitochondrial transcripts that encode the PC (EC 6.4.1.1) protein. The PC enzyme has 1,178 amino acids and contains three functional domains: biotin carboxylation, trans-carboxylation, and biotin carboxyl carrier<sup>[1]</sup>. This enzyme is a homotetramer consisting of four subunits, each subunit has a covalently attached biotin molecule and the binding sites for pyruvate, ATP, acetyl-CoA, and HCO<sub>3</sub>. PC facilitates a two-step reaction in the mitochondrial matrix. The first step is the ATP-dependent carboxylation of the biotin, which covalently binds to the BCCP, and the second step is the transfer of carboxyl group to pyruvate by biotin in the CT domain<sup>[2,3]</sup>. The PC enzyme forms oxaloacetate from pyruvate and HCO<sub>3</sub> in the mitochondrial matrix<sup>[4,5]</sup>. Mitochondrial oxaloacetate is a critical substrate for the Krebs cycle, gluconeogenesis, fatty acids, and protein biosynthesis<sup>[6]</sup>.

PCD (MIM#266150) is a rare metabolic disorder with a recessive mode of inheritance due to biallelic mutations in the *PC* gene. PCD manifests in three primary clinical forms: A or infantile (North American) type, B or neonatal (French) type, and C or benign type. Subtype B is the most severe form and presents in the first hours of birth, while subtype A becomes apparent several months after birth. Of note, subtype C is the mildest and late-onset form. In other words, types A and B are both early-onset, and almost all affected individuals die in infancy or early childhood<sup>[7,8]</sup>. In type B, the level of consciousness and neurological status are typical at birth. Nevertheless, following a metabolic derangement with hyperammonemia, hypoglycemia, hyper-citrullinemia, and lactic acidosis in the first hours, a hypokinetic-rigid syndrome occurs. This condition is associated with hypotonia, abnormal ocular movements, tremor of the limbs, and early death. In some patients, seizure and liver insufficiency develop in the first months of life, and patients die within a few months<sup>[9,10]</sup>. However, type A presents several months after birth with increasing hypotonia and generalized developmental delay, failure to thrive, profound apathy, and death in infancy or early childhood. In addition, patients may show intermittent lactic acidosis, especially during infections and other physiologic stresses<sup>[6,8]</sup>. On the other hands, type C is a late-onset and benign form that presents with recurrent episodes of ketoacidosis, mild psychological delay, and neurologic symptoms in infancy or early childhood<sup>[7,8]</sup>.

This study aimed to illustrate the genetic cause of metabolic disorders and early death in two newborns

admitted to the NICU for a metabolic decompensation. WES was carried out for the patients, and two novel variants were identified in the *PC* gene, one of which was classified as likely pathogenic and the other as VUS, according to the ACMG guidelines. The wild-type protein and the identified variants were modeled, and the effect of the variants on their secondary and tertiary structures was assessed. Moreover, the free energy of the normal protein and its interactions with ligands were scrutinized and compared with the novel (p.R156P) and a previously reported (p.R156Q) variant. Finally, the results of the evaluations provided evidence of pathogenicity for both identified variants, causing the early-onset form (type B PCD).

## MATERIALS AND METHODS

### Individuals

Two neonates (0003 and 0012 from the family No. 0003 and 0012), who were suspected of inherited metabolic disorders and admitted to the NICU of Ali-Asghar Pediatric Hospital, Tehran, Iran, were chosen for the study. Blood samples (5 ml) were taken from the neonates and available parents after performing pre-test genetic counseling.

### Sample collection and DNA extraction

DNA was extracted from blood samples using the QIAamp DNA Blood Mini Kit (Qiagen, Hilden, Germany) according to the manufacturer's instructions. The quantity and quality of DNA samples were evaluated by Thermo Scientific™ NanoDrop™ (1.8>A280/A260>2; Thermo Scientific, Waltham, MA, USA) and run on an agarose gel.

### Whole-exome sequencing

According to the clinical evaluations and initial biochemical tests, all the patients were suspected of an inherited metabolic disorder; hence, in addition to essential therapeutic approaches, WES was performed to accurately diagnose the genetic diseases. For this purpose, genomic DNA was fragmented, and all exons of protein-coding genes and flanking sequences were enriched using SureSelect Human All Exon V6 Kit (Agilent Technologies, Santa Clara, CA, USA). Subsequently, the generated library was sequenced on the NextSeq 500 platform (Illumina, San Diego, CA, USA) with an average coverage depth of 100×. After base calling, trimming the adapters, and FASTQ file quality controls, low-quality reads were eliminated. Next, reads were aligned to the reference human genome (hg19) using the Burrows-Wheeler Alignment tool<sup>[11]</sup>, and duplicates were removed via Picard tools

(<http://broadinstitute.github.io/picard>). Subsequently, variant calling was performed by the HaplotypeCaller tool, from Genome Analysis Toolkit version 4.0 (GATK4) package<sup>[12]</sup>. Annotation was then conducted by ANNOVAR<sup>[13]</sup> (<https://wannovar.wglab.org>), which extracts allele frequencies from known population databases, including the 1000 Genomes project (1000G, <http://www.internationalgenome.org>)<sup>[14]</sup>, the exome aggregation consortium (ExAC, <https://exac.broadinstitute.org>)<sup>[15]</sup>, genome aggregation database (gnomAD, <https://gnomad.broadinstitute.org>)<sup>[16]</sup>, and Kaviar dataset (<https://db.systemsbiology.net/kaviar/>)<sup>[17]</sup>. To predict pathogenicity and the potential effect of variants on protein structure and function as follows, we employed ANNOVAR using the datasets: SIFT (<https://sift.bii.a-star.edu.sg/>)<sup>[18]</sup>, PolyPhen-2 (<http://genetics.bwh.harvard.edu/pph2/>)<sup>[19]</sup>, Mutation Taster (<http://www.mutationtaster.org/>)<sup>[20]</sup>, PANTHER (<http://www.pantherdb.org/>)<sup>[21]</sup>, and PROVEAN (<http://provean.jcvi.org/>)<sup>[22]</sup>. After analyzing WES data, we used sequential filtering to select the most relevant variants. Then, considering the clinical symptoms, the following databases were used to exclude irrelevant variants: Online Mendelian Inheritance in Man (OMIM) (<https://www.omim.org/>), GeneReviews® (<https://www.ncbi.nlm.nih.gov/books/NBK1116/>), and Gene Cards (<https://www.genecards.org/>). At the end, the pathogenicity of the final variants was evaluated in ClinVar (<https://www.ncbi.nlm.nih.gov/clinvar/>), dbSNP (<https://www.ncbi.nlm.nih.gov/snp/>), InterVar (<http://wintervar.wglab.org/>), and Varsome (<https://varsome.com/variant/hg19/>)<sup>[23]</sup> datasets. Besides, to assess the allele frequency of the final variants in Iranian ethnicity, Iranome (<http://www.iranome.com>) database was utilized.

### Confirmatory analysis by Sanger sequencing

Variants identified in the neonates and the available parents were confirmed through Sanger sequencing. Primer sequences are presented in [Supplementary Table 1](#). Finally, the pathogenicity of the variants was evaluated according to the ACMG guidelines<sup>[24]</sup>.

### Modeling and protein structure analysis

#### Sequence and structure of proteins

The PC sequence was retrieved from the UniprotKB database (ID: P11498; <https://www.uniprot.org/uniprotkb/>) and submitted to SWISS-MODEL for model building. The homology modeling pipeline identifies target-template proteins based on BLAST (<https://blast.ncbi.nlm.nih.gov/Blast.cgi>) and HHblits (<https://toolkit.tuebingen.mpg.de/tools/hhblits>). The resulting models were ranked based on GMQE, a dataset indicating the quality of the models<sup>[25]</sup>. In addition,

homology modeling for the frameshift variant c.908delG:p.G303Afs\*40 was performed by the I-TASSER server (<https://zhanggroup.org/I-TASSER/>) for subsequent comparison with wild-type PC.

#### Evaluation of the SNP effects on the protein secondary and tertiary structure

The PSIPRED server (<http://bioinf.cs.ucl.ac.uk/psipred/>) was utilized to predict the secondary structure of wild-type and mutant (R156Q and R156P) proteins<sup>[26,27]</sup>. Furthermore, 3D structures of the mutant proteins were generated using Chimera (version 1.8)<sup>[28]</sup>. To remove atomic clashes of the protein structure, energy minimization was implemented in 100 steps (step size = 0.02 Å) using AMBER f12SB force field parameters and the steepest descent and conjugate gradient algorithms. The functional form of the PC enzyme is known as a homotetramer that interacts with the ligands ATP, biotin, and pyruvate. Hence, in the wild-type and PC variants modeling, the studied monomer format was in complex with ATP. This behavior was due to the position of mutations R156P and R156Q in the ATP binding domain. Finally, the binding affinity of proteins and ligands was calculated and compared using the PRODIGY server (<https://wenmr.science.uu.nl/prodigy/>)<sup>[29]</sup>.

#### Prediction of protein structure flexibility

Amino acid fluctuations were predicted during coarse-grained simulation using the CABS-flex web server (<http://biocomp.chem.uw.edu.pl/CABSflex/>)<sup>[30]</sup>. The residue fluctuation profile was generated as an interactive 2D plot displaying the RMSF of the amino acids during the simulation. Protein structures were uploaded as PDB format files, and the simulations were performed with default parameters.

#### Prediction of functional SNPs effect by PolyPhen-2

PolyPhen-2 estimates the possible effect of residue replacement using supervised machine learning. It predicts the probability for a mutation to be damaged based on the information of the protein sequence, phylogenetics, and structure. PolyPhen-2 uses datasets HumDiv and HumVar from the UniProtKB database for training and testing the predicted models. HumDiv contains collections of human Mendelian disease-causing mutations and differences between homologous human and mammalian proteins with non-deleterious effects, while HumVar includes all pathogenic and non-pathogenic human SNPs<sup>[19]</sup>.

#### Prediction of the functional SNP effect by SNAP2

SNAP2 (<https://roslab.org/services/snap2web/>) server was used to evaluate the functional outcome of

R156 substitutions with either P or Q on PC protein. The SNAP2 score was calculated according to the data of multiple sequence alignments, secondary structure, and solvent accessibility of the protein sequence using the neural network method<sup>[31]</sup>.

#### **Prediction of the functional consequence of SNPs by SNPs&GO**

SNPs&GO (<http://snps.biofold.org/snps-and-go>) predicts whether the single amino acid substitution affects the function of a protein. Using a sequence-based algorithm, SNPs&GO calculates the pair-wise alignments with the BLAST algorithm against the UniRef90 dataset to generate the sequence profile. The probability for mutations to be damaging is calculated using sequence feature data, frequency data of different residues as the sequence environment, and the functional annotation score related to gene ontology terms. However, in the structure-based algorithm, SNPs&GO uses the structural environment and relative solvent-accessible region data for the wild-type amino acid<sup>[32]</sup>.

#### **Prediction of protein stability by I-Mutant 2.0**

The PC stability changes were predicted based on the protein sequence and structure using I-Mutant 2.0 server acting based on a support vector machine tool<sup>[33]</sup>. The impact of mutation was evaluated by calculating the change in the free energy value ( $\Delta\Delta G$ ) of the protein. A positive  $\Delta\Delta G$  value indicates increased stability of the protein, and a  $\Delta\Delta G$  more than 0.5 suggests significant stability; however, a negative  $\Delta\Delta G$  value represents decreased stability. The values of the reliability index ranged from 0 to 10.

#### **Prediction of functional, molecular, and phenotypic effects of SNPs by FATHMM**

FATHMM server is a sequence evolutionary-based tool that predicts the functional influence of SNVs on protein. The computational prediction uses Hidden Markov Models to evaluate the sequence conservations by aligning homologous sequences in an unweighted/species-independent method<sup>[34]</sup>. A negative score indicates the probable damaging effects of an amino acid substitution.

## **RESULTS**

### **Clinical features of the disease**

The probands (neonates 0003 and 0012) were the results of consanguineous marriages with no family history of similar conditions. In both neonates, the disease started at the first day of the life, and they deceased in a couple of days. The results of first level-

biochemical tests demonstrated hypoglycemia, hyperammonemia, lactic acidosis, and disturbed LFT tests in both patients, suggesting a metabolic disorder. However, no definitive diagnosis was possible, and the patients died before the diagnostic workup was completed.

### **WES and mutation detection**

In patient 0003, WES data analysis revealed a novel homozygous missense variant, c.467G>C, p.R156P, NM\_000920.4, in exon 5 of the PC gene related to PCD (MIM#266150). Sanger sequencing successfully confirmed the genotypes in the proband and his parents (Fig. 1A). According to the ACMG guidelines, this variant was categorized as a VUS<sup>[23,24]</sup>. In patient 0012, the novel homozygous frameshift variant, c.908del, p.G303Afs\*40, NM\_000920.4, was detected in exon 9 of the PC gene, which was confirmed by Sanger sequencing (Fig. 1B). However, it was impossible to confirm the parents' heterozygous genotype due to the unavailability of blood samples. In accordance with the ACMG guidelines, this variant was categorized as likely pathogenic<sup>[23,24]</sup>. Given the recent recommendation about PP3<sup>[35-37]</sup>, the variant c.467G>C, p.R156P, having PP3, PM2, and PM5 criteria, and the variant c.908del, p.G303Afs\*40, with PVS1, PM2, and PP5 criteria, are classified as likely pathogenic, and pathogenic variants, respectively. In addition, according to the patient's phenotype, clinical presentation, and parental consanguinity, both variants get PP4 criterion in both patients.

### **Homology modeling and protein structure analysis**

#### **Modeling the protein 3D structure**

The canonical isoform of PC and its functional domains are depicted in Figure 2A. The crystal structure of *Staphylococcus aureus* PC (3BG5) was proposed as a template for modeling. This template had 48.86% sequence identity and 43% sequence similarity with human PC<sup>[38]</sup>. The GMQE score between 0 and 1 indicates an overall quality estimation based on the template coverage (Table 1). The crystal structure of the biotin carboxylase PC (2DZD) domain was used for modeling the frameshift mutant by SWISS-MODEL, where it shares 58.06% and 47% sequence identity and similarity, respectively, with input sequence<sup>[39]</sup>. The crystal structure of biotin carboxylase from *Staphylococcus aureus* (2VPQ) was the top template proposed by I-TASSER to model the PC frameshift variant<sup>[40]</sup>. In the I-TASSER output, the models are ranked by c-score, which indicates the overall quality of the predicted models, from -5 to 2. Higher values in c-score indicate higher modeling accuracy. Comparing two proposed structures for the PC frameshift mutation indicated the complete coverage of the I-TASSER

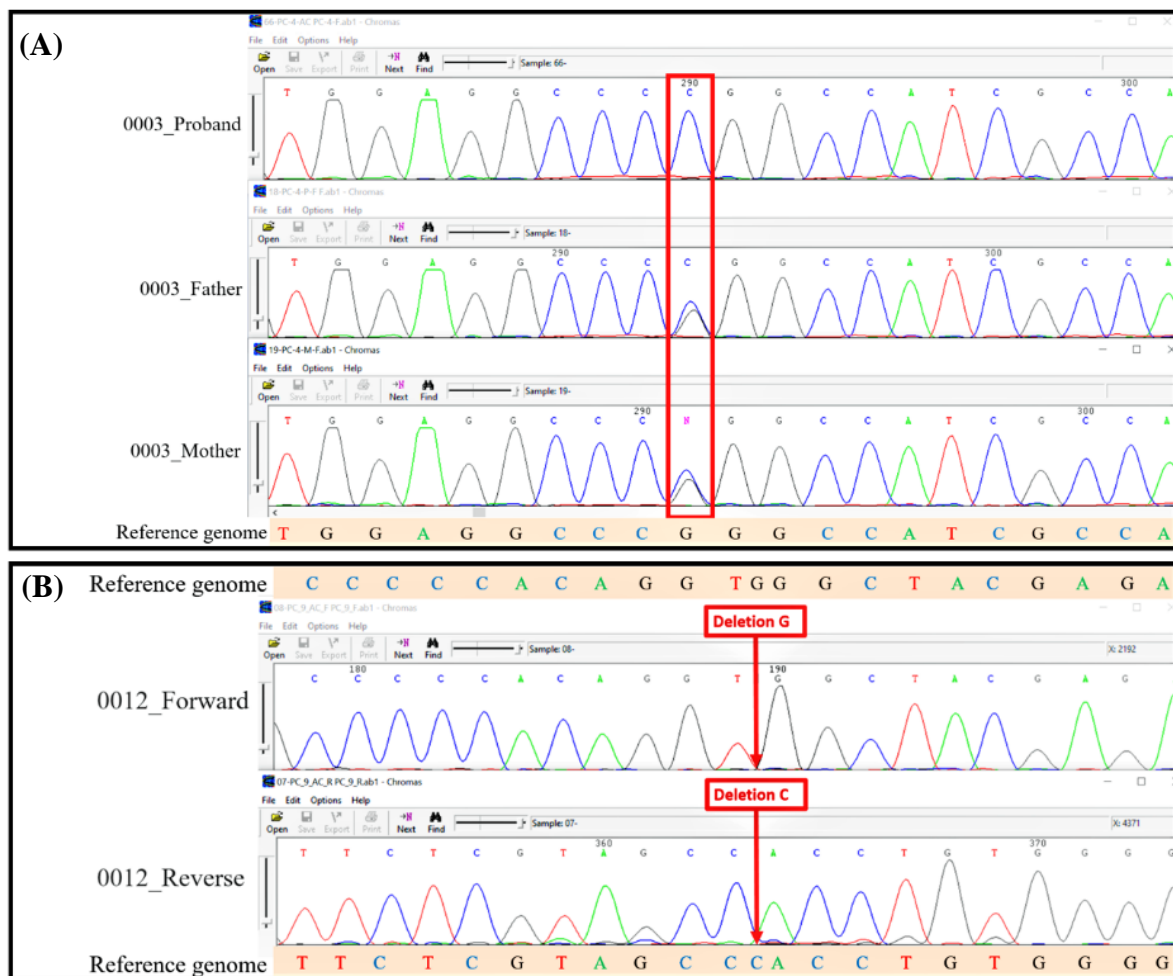


**Fig. 1.** Sanger sequencing electropherograms. (A) Sanger sequencing confirmed the homozygous status of the proband 0003 (above) for the missense variant of c.467G>C and the heterozygous state of his father (middle) and mother (below); (B) Sanger sequencing results confirmed the homozygous c.908del frameshift variant in proband 0012 with the input sequences.

model with 341 amino acids, while SWISS-MODEL presented a 276-amino acid model for residues 34-310 (Fig. 2B and 2C). Alignment of the two models showed RMSD of 0.721Å. Differences in the models in terms of 3D conformation are in yellow (Fig. 2D). The missing domains of the PC frameshift variant models compared to the wild-type PC are depicted in Figure 2E.

#### *SNV effects on secondary and tertiary structure of protein*

The secondary structure of wild-type PC and its variants was evaluated by PSIPRED. Although only one residue was changed, slight differences were predicted for the 2D form of the R156P variant. However, the secondary structure around the substituted residues, either P156 or Q156, showed no variation compared to the wild-type residue (R156). Differences in the predicted secondary structure of wild-type PC and variants (residues 1-400) are designated in Figure 3A,

3B, and 3C. Secondary structure prediction of the G303A PC frameshift mutant indicated several variations compared to the wild-type PC. The most significant difference was observed in the protein sequence after the mutation site G303A, where the sequence was completely changed. This includes the R328, a critical amino acid in ATP binding, which was replaced by alanine (Fig. 3D and 3E). Since the R156P and R156Q mutations are located in the ATP-grasp domains of PC, the effect of SNVs on the 3D structure was evaluated based on the interactions of the proteins with ATP ligand. The wild-type PC and ATP interaction pattern indicated residues K194, E236, R328, and T478. Residue profile in PC-R156Q and ATP interaction was composed of E236, R328, and Y321, while in PC-R156P consisted of K194, Y197, E236, and Q268 (Table 2). The binding affinity of proteins and ATP indicated a higher tendency of wild-type PC to ATP than the variants (Fig. 4).

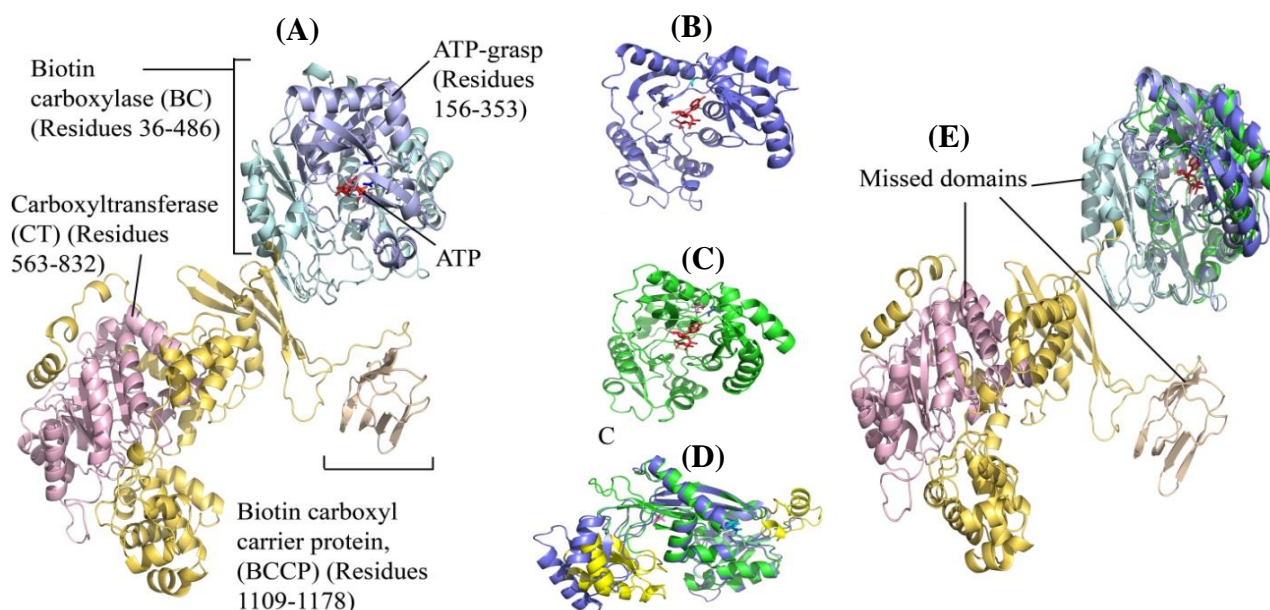


**Fig. 2.** Cartoon view of PC protein and PC frameshift variant models. (A) Domains of PC protein by focusing on ATP-grasp domain; PC frameshift variant modeled by SWISS-MODEL (B) and I-TASSER (C); (D) Structural alignment of PC frameshift variant models where the differences are yellow colored; (E) Structural alignment of PC frameshift variants models and wild-type PC showing missing domains.

### Generation of residue fluctuation profile

Residue fluctuation profiles were generated as the RMSF plots of amino acids during the simulations of wild-type and variants PCs (Fig. 5A and 5B). A close-up view of the fluctuations in the ATP-binding domain (residues 150-350) is displayed in Figure 5B. In spite of no significant change in the fluctuations of residues 156 and 328, which are critical in ATP binding, other residues in the ATP binding domains displayed variations, showing different affinities to ATP. On the other hand, residues in both frameshift variant models showed relatively similar fluctuations (Fig. 5C). Since the sequence of PC frameshift has changed from residue 303, a different fluctuation pattern was detected at the C-terminal compared to the wild-type PC protein.

### Analysis of SNP effects by Polyphen-2 and SNAP2

The SNAP2 server predicted SNVs R156P and R156Q as functionally effective mutations with 91% and 95% accuracy and scores of 84 and 97, respectively (Table 3). The scores ranged from -100 to +100, showing “strong neutral” and “strong effect” on protein function, respectively. A heatmap representation of residues 123-178 is depicted in Figure 6A, indicating the high impact of R156 substitutions. Polyphen-2 scores predicted the R156P and R156Q variants as “damaging” (Table 3). Likewise, the HumDiv and HumVar indicators are located in the red zone (Fig. 6B and 6C), indicating both variants were damaging.

**Table 1.** Homology modeling of proteins using SWISS-MODEL and I-TASSER

Protein	Template PDB ID	Sequence identity (%)	Sequence similarity (%)	Coverage	GMQE	C-score
PC	3BG5	48.86	43	0.96 (36-1178)	0.71	-
PC* (frameshift mutation)	2DZD	58.06	47	0.84 (34-310)	0.70	-
PC** (frameshift mutation)	2VPQ	48	-	0.87 (37-337)	-	-0.06

\*modelled by SWISS-MODEL; \*\*modelled by I-TASSER

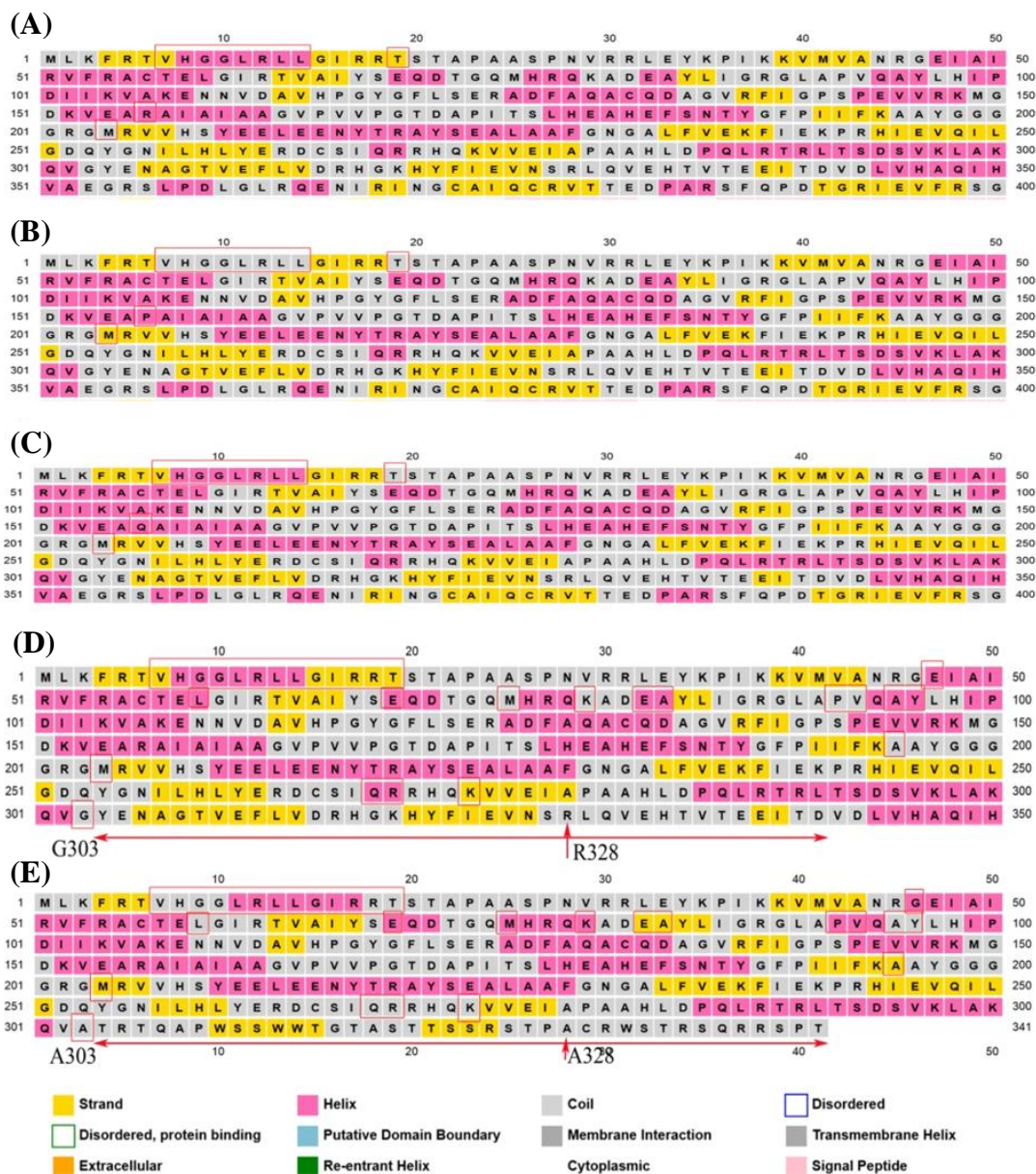


**Fig. 3.** The secondary structure prediction of wild-type PC and variants. (A) Wild-type PC protein (residues 1-400); (B) PC-R156P protein; (C) PC-R156Q protein; (D) Wild-type PC protein (residues 1-350); (E) PC frameshift variant.

**Table 2.** Evaluation of SNP effects on binding affinity and interactions

Protein	$\Delta G$	ATP residues in interaction
Wild-type PC	-7.6	K194, E236, R328, T478
PC-R156Q	-7.2	E236, R328, Y321
PC-R156P	-7.1	K194, Y197, E236, Q268

### Prediction of mutation effect using I-Mutant 2.0, FATHMM, and SNPs&GO servers

PC stability changes due to the SNVs were evaluated by I-Mutant 2.0 according to the protein sequence and

structure, which are summarized in Table 3. Since negative  $\Delta\Delta G$  scores represent decreased protein stability, the data revealed a destabilizing effect of both variants on PC protein. Furthermore, SNP analysis by FATHMM calculated negative scores (-4.59 and -4.57 for R156P and R156Q, respectively), indicating a damaging effect of R156P and R156Q on PC protein. In addition, the SNPs&GO predicted both mutations as disease-causing with a probability greater than 0.5 (Table 3).

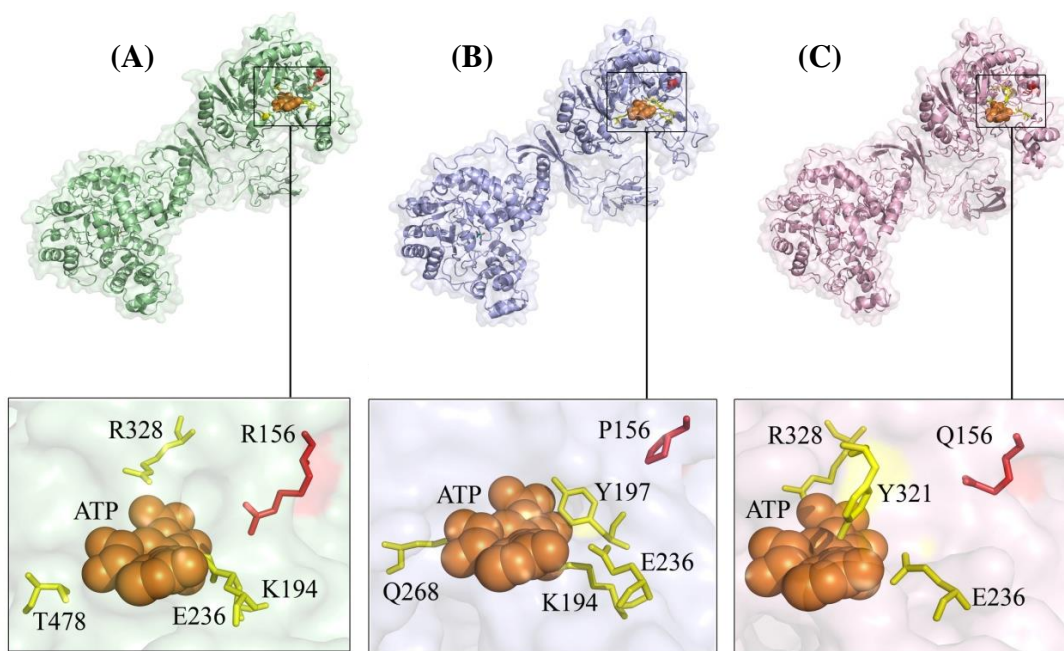


**Fig. 4.** The tertiary structure of PC protein and its variants complex with ATP. (A) Wild-type PC protein and residues involved in the interaction with ATP; R156P (B) and R156Q (C) proteins and residues involved in the interaction with ATP.

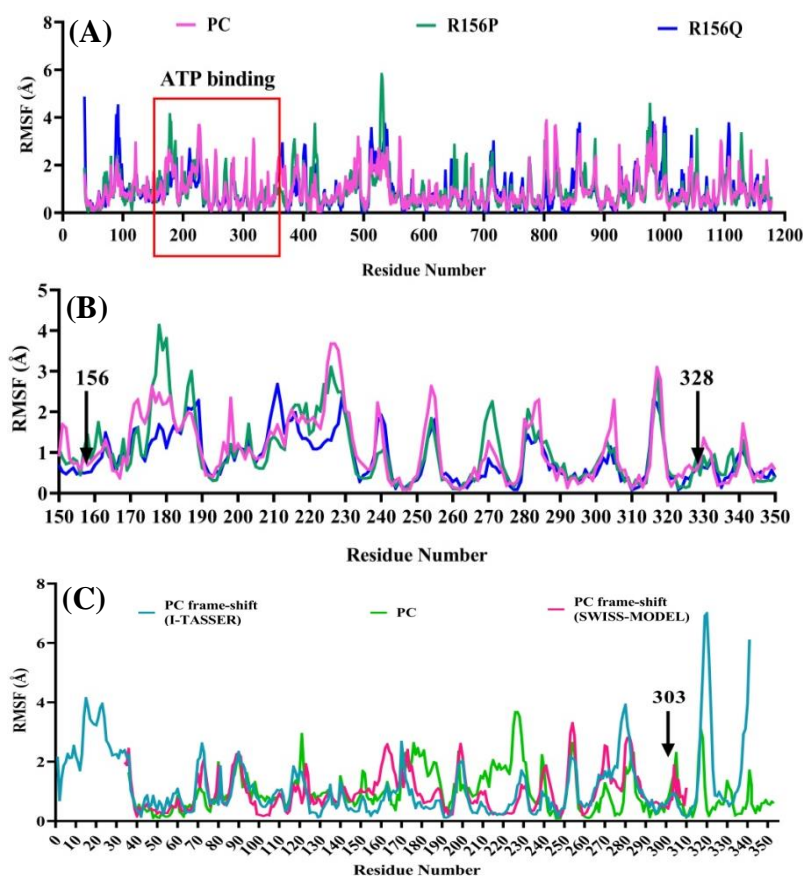


**Fig. 5.** RMSF plot of residues during the simulation. (A) PC protein and its variants (R156P and R156Q); (B) Close-up view of fluctuations in the ATP-binding domain (~150-350); (C) RMSF plot of PC frameshift variant models by I-TASSER and SWISS-MODEL compared to PC protein.



**Table 3.** Evaluation of SNP effects on PC protein

Variant	Polyphen-2		Prediction	SNAP2		SNPs&GO (sequence)		
	Score	HumVar		Score	Prediction	Probability	Prediction	RI
R156Q	0.991	0.919	Damaging	97	Effect	0.639	Disease	3
R156P	0.995	0.998	Damaging	84	Effect	0.893	Disease	8

Variant	I-Mutant		ΔAG (kcal/mol) (structure)	FATHMM		SNPs&GO		
	ΔAG (kcal/mol) (sequence)	Stability prediction		Score	Prediction	Probability	Prediction	RI
R156Q	-0.7	Decrease	-1.29	-4.57	Damaging	0.896	Disease	8
R156P	-0.55	Decrease	-1.28	-4.59	Damaging	0.956	Disease	9

RI, reliability index

## DISCUSSION

In the present study, WES revealed that patients 0003 and 0012 were homozygous for the novel variants c.467G>C (p.R156P) in exon 5 and c.908del (p.G303Afs\*40) in exon 9 of the *PC* gene, respectively. Both variants were confirmed by Sanger sequencing in the probands and available parents. According to the ACMG guidelines<sup>[24]</sup> and recent statement about PP3 criteria<sup>[35-37]</sup>, the variant in patient 0003, c.467G>C (p.R156P), is likely pathogenic, and that in patient 0012, c.908del (p.G303Afs\*40), is a pathogenic variant. In addition, based on the patient's clinical presentation and parental consanguinity, both variants received an additional PP4 score. Interestingly, Wang et al.<sup>[8]</sup> reported another variant, c.467G>A (p.R156Q), at position 156, which has been reported to be a VUS in ClinVar<sup>[8]</sup>, and seems to be likely pathogenic in VarSome (2022)<sup>[23]</sup>, and pathogenic in UniProt<sup>[7]</sup>. In

patient 0012, the frameshift variant c.908del induced an aberrant stop codon after the addition of 40 amino acids and activation of the nonsense-mediated mRNA decay mechanism. This variant changes the protein active site and eliminates the crucial functional domains, such as pyruvate carboxyltransferase and biotin-binding domains, as well as disrupts the biotin carboxylation and ATP grasp domains (Fig. 7).

Currently, 62 disease-causing variants, including 42 missense/nonsense, 7 splicings, 7 small deletions, 5 small insertions, and 1 minor duplication, have been reported for the *PC* gene in HGMD Professional 2021.4 (<https://www.hgmd.cf.ac.uk/ac/gene.php?gene=PC>). Tsygankova et al.<sup>[41]</sup> have reported four exonic variants, one chromosomal translocation, and one deep intronic variant related to PCD. The present study suggests two additional pathogenic variants, c.467G>C and c.908del, to expand the *PC* variants spectrum (Fig. 7).

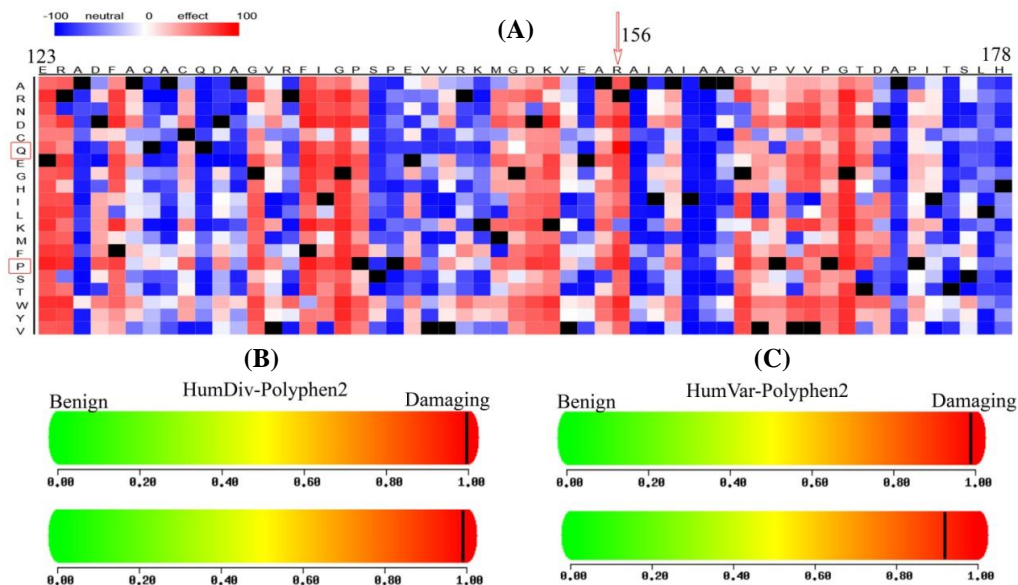


**Fig. 6.** Prediction of SNP effect on PC protein. (A) Heatmap by SNAP2 (residues 123-178); HumDiv (B) and HumVar (C) results for R156P (above) and R156Q (below) substitutions.

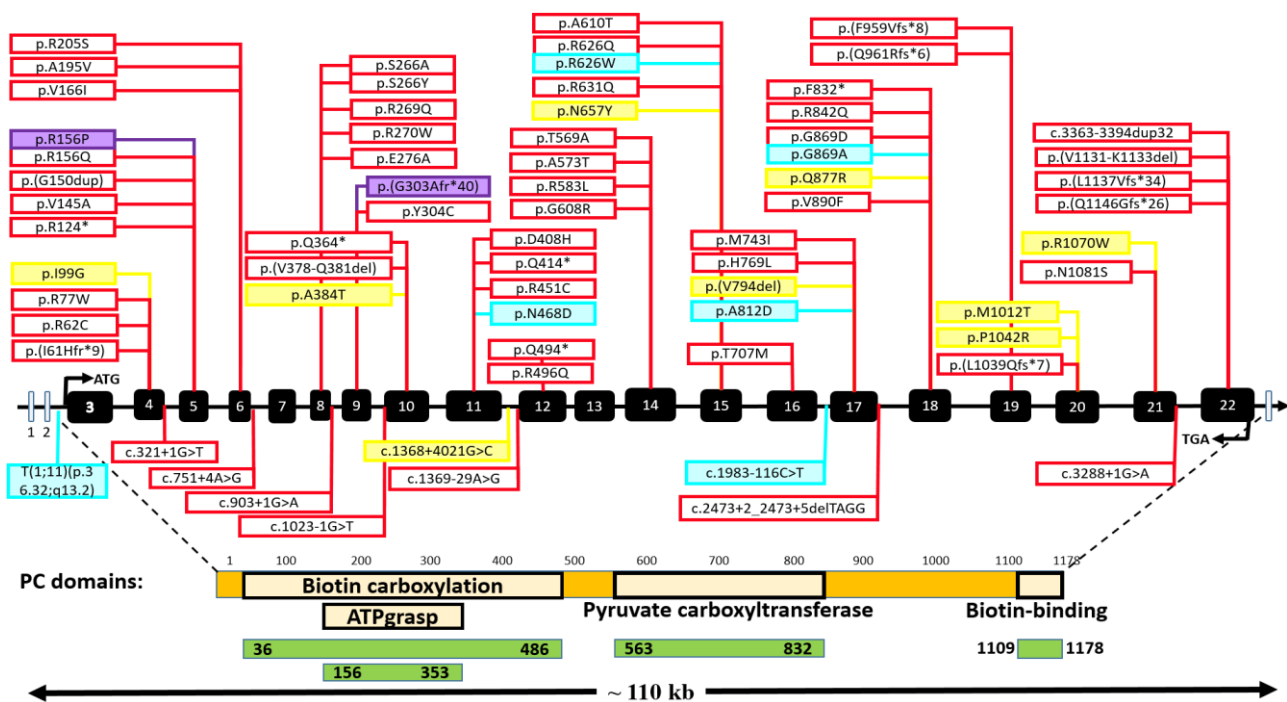


**Fig. 7.** Review of the reported *PC* gene variants. Exonic and intronic variants are shown above and below the *PC* gene, respectively. Red boxes: deleterious variants published in HGMD professional (ver.2022.2) (<https://www.hgmd.cf.ac.uk/ac/gene.php?gene=PC>); yellow boxes: variants of uncertain significance, according to HGMD (ver.2022.2); blue boxes: novel variants reported by Tsygankova et al.<sup>[41]</sup>; violet boxes: suggested variants in the present study.

Surprisingly, few variants have been reported in this gene, which might be due to the early-onset and lethal nature of forms A and B of the PCD<sup>[7,8]</sup>.

PCD (MIM#266150) is a rare autosomal recessive disorder resulting from biallelic mutations in the *PC* gene (<https://www.ncbi.nlm.nih.gov/gene/5091>). The high frequency of consanguineous marriages in countries like Iran can increase the prevalence of rare autosomal recessive disorders<sup>[42-44]</sup>. However, there are few reports of PCD in the Iranian population. Bayat et al.<sup>[45]</sup> have reported a two-year-old girl from Iran with c.806G>A variant in the *PC* gene and a longer survival<sup>[45]</sup>. All patients in the present and previous studies were resulted from consanguineous marriages. PCD manifests in three primary clinical forms, A, B, and C. Unlike early onset types A and B, patients with type C often survive until late adolescence<sup>[8]</sup>. According to the biochemical test results, clinical course, and disease survival, the patients in this study seem to be affected by type B PCD. PC enzyme activity in fibroblasts culture is a well-known indicator for PCD diagnosis in newly diagnosed patients<sup>[8]</sup>, though it cannot indicate the extent of PC activity impairment<sup>[3]</sup>. However, PC enzyme assay and fibroblast culture are inaccessible in Iran.

An earlier study has indicated that pathogenic missense variants typically belong to the 2/3 N-terminal

end of the PC. On the other hand, mutations in the 1/3 C-terminal end are tolerable and unlikely to cause disease<sup>[7]</sup>. Furthermore, it has been reported that at least one truncating variant leads to type B and a neonatal-fatal form of PCD, while homozygous missense variants are the genetic cause of type A PCD<sup>[7, 10]</sup>. In complete agreement with Monnot et al.'s<sup>[7]</sup> and Carbone et al.'s<sup>[10]</sup> investigations, our study revealed that the patient 0012 was homozygous for the truncating variant c.908del, p.G303Afs\*40 related to type B PCD. However, the causative mutations of all type B patients are not nonsense; there are reports of biallelic missense variants in patients presenting type B PCD<sup>[8,46,47]</sup>. Likewise, one of the patients in this study who expired from type B PCD in the neonatal period, inherited the homozygous missense variant c.467G>C, p p.R156P. However, Monnot et al.<sup>[7]</sup> reported the variant p.R156Q for the first time as a cause of type A PCD. Nevertheless, the genotype/phenotype correlations in type A and C PCD have not fully been elucidated, since both types have been observed with biallelic missense mutations<sup>[3]</sup>. Recently, in silico free energy calculations have increasingly been used to evaluate the effect of residue substitutions on protein structure, stability, and ligand binding affinity<sup>[43,48-52]</sup>. In 2019, Coci et al.<sup>[3]</sup> estimated the stability of variant PCs by calculating the double free energy difference ( $\Delta\Delta G$ ). They reported that p.R156 is

a residue close to the ATP binding site, and the variant p.R156Q in the protein biotin carboxylation domain destabilizes the PC structure. In complete accordance with Coci et al.<sup>[3]</sup>, our free energy calculations exhibited a destabilized PC due to p.R156Q and p.R156P. Moreover, protein and ligand binding affinity evaluations indicated a higher affinity of wild-type PC to ATP than their variants (Fig. 4).

WES data analysis, confirmatory Sanger sequencing, pathogenicity evaluations according to ACMG guidelines, and in silico protein assessments revealed a novel missense variant, c.467G>C, p.R156P, in patient 0003 and a novel frameshift variant, c.908del, p.G303Afs\*40, in patient 0012, which both are suggested to be pathogenic relating to type B PCD. However, more studies with larger sample sizes and functional analysis are necessary to be carried out to confirm these observations. The results of this study could expand the variant spectrum for the PC gene and would be helpful for pediatricians, endocrinologists, geneticists, scientists, and the patients' families. In addition, in the cases of VUS variants, homology modeling and in silico analysis of the effects of variants on protein stability and ligand interactions can improve the pathogenicity score of the variants.

## DECLARATIONS

### Acknowledgments

The authors appreciate the patients' families for their participation and the NICU staff (academic members, fellowships, residents, and nurses) of Ali-Asghar Pediatrics Hospital (Tehran, Iran) for their helpful cooperation. The authors also thank the employees of the Molecular Medicine Department, Pasteur Institute of Iran, Tehran, Iran, for their unique and friendly collaborations.

### Ethical statement

The protocol of this study was authorized and approved by the Ethics Committee of the Pasteur Institute of Iran (ethical code: IR.PII.REC.1397.70). All the participants gave their informed consents.

### Data availability

For patients' confidentiality reasons, data related to WES is available by reasonable requests from the corresponding author.

### Author contributions

FM: wrote the concept of the study, designed the experiments, collected samples, performed the laboratory assessment, and analyzed and interpreted the

data and prepared the initial draft of the paper; ER: performed the laboratory assessment and analyzed and interpreted the data and prepared the initial draft of the paper; EDD: revised the manuscript; NK: collected samples, wrote the concept of the study, and designed the experiments; ST: wrote the concept of the study; RM: provided materials and equipment and gave helpful advice at every stage; SZ: wrote the concept of the study, designed the experiments, and revised the manuscript. The study was carried out under the supervision of SZ and NK. All authors read and commented on the manuscript.

### Conflict of interest

None declared.

### Funding/support

This work is a partial fulfillment of the Ph.D. thesis of Mrs. Fereshteh Maryami under supervision of Professor Sirous Zeinali and was financially supported by The Deputy of Research and Technology, Pasteur Institute of Iran, Tehran, Iran.

## REFERENCES

- Wallace JC, Jitrapakdee S, Chapman-Smith A. Pyruvate carboxylase. *The international journal of biochemistry and cell biology* 1998; **30**(1): 1-5.
- Wexler ID, Kerr DS, Du Y, Kaung MM, Stephenson W, Lusk MM, Wappner RS, Higgins JJ. Molecular characterization of pyruvate carboxylase deficiency in two consanguineous families. *Pediatric research* 1998; **43**(5): 579-584.
- Coci EG, Gapsys V, Shur N, Shin-Podskarbi Y, de Groot BL, Miller K, Vockley J, Sondheimer N, Ganetzky R, Freisinger P. Pyruvate carboxylase deficiency type A and type C: Characterization of five novel pathogenic variants in PC and analysis of the genotype-phenotype correlation. *Human mutation* 2019; **40**(6): 816-827.
- Lee SH, Davis EJ. Carboxylation and decarboxylation reactions. Anaplerotic flux and removal of citrate cycle intermediates in skeletal muscle. *The journal of biological chemistry* 1979; **254**(2): 420-430.
- Crabtree B, Higgins SJ, Newsholme EA. The activities of pyruvate carboxylase, phosphoenolpyruvate carboxylase and fructose diphosphatase in muscles from vertebrates and invertebrates. *Biochemical journal* 1972; **130**(2): 391-396.
- Marin-Valencia I, Roe CR, Pascual JM. Pyruvate carboxylase deficiency: mechanisms, mimics and anaplerosis. *Molecular genetics and metabolism* 2010; **101**(1): 9-17.
- Monnot S, Serre V, Chadeaux-Vekemans B, Aupetit J, Romano S, De Lonlay P, Rival JM, Munnich A, Steffann J, Bonnefont JP. Structural insights on pathogenic effects of novel mutations causing pyruvate carboxylase deficiency. *Human mutation* 2009; **30**(5): 734-740.
- Wang D, Yang H, De Braganca KC, Lu J, Shih LY,

- Briones P, Lang T, De Vivo DC. The molecular basis of pyruvate carboxylase deficiency: mosaicism correlates with prolonged survival. *Molecular genetics and metabolism* 2008; **95**(1-2): 31-38.
9. Carbone, M.A., D.A. Applegarth, and B.H. Robinson. Intron retention and frameshift mutations result in severe pyruvate carboxylase deficiency in two male siblings. *Human mutation* 2002; **20**(1): 48-56.
  10. Carbone MA, MacKay N, Ling M, Cole DE, Douglas C, Rigat B, Feigenbaum A, Clarke JT, Haworth JC, Greenberg CR, Seargeant L, Robinson BH. Amerindian pyruvate carboxylase deficiency is associated with two distinct missense mutations. *American journal of human genetics* 1998; **62**(6): 1312-1319.
  11. Li H, Durbin R. Fast and accurate short read alignment with Burrows-Wheeler transform. *Bioinformatics* 2009; **25**(14): 1754-1760.
  12. DePristo MA, Banks E, Poplin R, Garimella KV, Maguire JR, Hart C, Philippakis AA, del Angel G, Rivas MA, Hanna M, McKenna A, Fennell TJ, Kernysky AM, Sivachenko AY, Cibulskis K, Gabriel SB, Altshuler D, Daly MJ. A framework for variation discovery and genotyping using next-generation DNA sequencing data. *Nature genetics* 2011; **43**(5): 491-498.
  13. Wang K, Li M, Hakonarson H. ANNOVAR: functional annotation of genetic variants from high-throughput sequencing data. *Nucleic acids research* 2010; **38**(16): e164.
  14. 1000 Genomes Project Consortium, Abecasis GR, Altshuler D, Auton A, Brooks LD, Durbin RM, Gibbs RA, Hurles ME, McVean GA. A map of human genome variation from population-scale sequencing. *Nature* 2010; **467**(7319): 1061-1073.
  15. Lek M, Karczewski KJ, Minikel EV, Samocha KE, Banks E, Fennell T, O'Donnell-Luria AH, Ware JS, Hill AJ, Cummings BB, Tukiainen T, Birnbaum DP, Kosmicki JA, Duncan LE, Estrada K, Zhao F, Zou J, Pierce-Hoffman E, Berghout J, Cooper DN, Deflaux N, DePristo M, Do R, Flannick J, Fromer M, Gauthier L, Goldstein J, Gupta N, Howrigan D, Kiezun A, Kurki MI, Moonshine AL, Natarajan P, Orozco L, Peloso GM, Poplin R, Rivas MA, Ruano-Rubio V, Rose SA, Ruderfer DM, Shakir K, Stenson PD, Stevens C, Thomas BP, Tiao G, Tusie-Luna MT, Weisburd B, Won HH, Yu D, Altshuler DM, Arduessino D, Boehnke M, Danesh J, Donnelly S, Elosua R, Florez JC, Gabriel SB, Getz G, Glatt SJ, Hultman CM, Kathiresan S, Laakso M, McCarroll S, McCarthy MI, McGovern D, McPherson R, Neale BM, Palotie A, Purcell SM, Saleheen D, Scharf JM, Sklar P, Sullivan PF, Tuomilehto J, Tsuang MT, Watkins HC, Wilson JG, Daly MJ, MacArthur DG; Exome Aggregation Consortium. Analysis of protein-coding genetic variation in 60,706 humans. *Nature* 2016; **536**(7616): 285-291.
  16. Havrilla JM, Pedersen BS, Layer RM, Quinlan AR. A map of constrained coding regions in the human genome. *Nature genetics* 2019; **51**(1): 88-95.
  17. Glusman G, Caballero J, Mauldin DE, Hood L, Roach JC. Kaviar: an accessible system for testing SNV novelty. *Bioinformatics* 2011; **27**(22): 3216-3217.
  18. Ng PC, Henikoff S. SIFT: Predicting amino acid changes that affect protein function. *Nucleic acids research* 2003; **31**(13): 3812-4.
  19. Adzhubei IA, Schmidt S, Peshkin L, Ramensky VE, Gerasimova A, Bork P, Kondrashov AS, Sunyaev SR. A method and server for predicting damaging missense mutations. *Nature methods* 2010; **7**(4): 248-249.
  20. Schwarz JM, Cooper DN, Schuelke M, Seelow D. MutationTaster2: mutation prediction for the deep-sequencing age. *Nature methods* 2014; **11**(4): 361-362.
  21. Mi H, Guo N, Kejariwal A, Thomas PD. PANTHER version 6: protein sequence and function evolution data with expanded representation of biological pathways. *Nucleic acids research* 2007; **35**(Database issue): D247-D252.
  22. Choi Y, Chan AP. PROVEAN web server: a tool to predict the functional effect of amino acid substitutions and indels. *Bioinformatics* 2015; **31**(16): 2745-2747.
  23. Kopanos C, Tsiolkas V, Kouris A, Chapple CE, Aguilera MA, Meyer R, Massouras A. VarSome: the human genomic variant search engine. *Bioinformatics* 2019; **35**(11): 1978-1980.
  24. Richards S, Aziz N, Bale S, Bick D, Das S, Gastier-Foster J, Grody WW, Hegde M, Lyon E, Spector E, Voelkerding K, Rehml HL, ACMG Laboratory Quality Assurance Committee. Standards and guidelines for the interpretation of sequence variants: a joint consensus recommendation of the American College of Medical Genetics and Genomics and the Association for Molecular Pathology. *Genetics in medicine* 2015; **17**(5): 405-424.
  25. Waterhouse A, Bertoni M, Bienert S, Studer G, Tauriello G, Gumienny R, Heer FT, de Beer TAP, Rempfer C, Bordoli L, Lepore R, Schwede T. SWISS-MODEL: homology modelling of protein structures and complexes. *Nucleic acids research* 2018; **46**(W1): W296-W303.
  26. Buchan DWA, Jones DT. The PSIPRED protein analysis workbench: 20 years on. *Nucleic acids research* 2019; **47**(W1): W402-W407.
  27. McGuffin LJ, Bryson K, Jones DT. The PSIPRED protein structure prediction server. *Bioinformatics* 2000; **16**(4): 404-405.
  28. Pettersen EF, Goddard TD, Huang CC, Couch GS, Greenblatt DM, Meng EC, Ferrin TE. UCSF Chimera--a visualization system for exploratory research and analysis. *Journal of computational chemistry* 2004; **25**(13): 1605-12.
  29. Xue LC, Rodrigues JP, Kastritis PL, Bonvin AM, Vangone A. PRODIGY: a web server for predicting the binding affinity of protein-protein complexes. *Bioinformatics* 2016; **32**(23): 3676-3678.
  30. Kuriata A, Gierut AM, Oleniecki T, Ciemny MP, Kolinski A, Kurcinski M, Kmiecik S. CABS-flex 2.0: a web server for fast simulations of flexibility of protein structures. *Nucleic acids research* 2018; **46**(W1): W338-W343.
  31. Hecht M, Bromberg Y, Rost B. Better prediction of functional effects for sequence variants. *BMC genomics* 2015; **16** Suppl 8 (Suppl 8): S1.

32. Capriotti E, Calabrese R, Fariselli P, Martelli PL, Altman RB, Casadio R. WS-SNPs&GO: a web server for predicting the deleterious effect of human protein variants using functional annotation. *BMC genomics* 2013; **14** (Suppl 3): S6.
33. Capriotti E, Fariselli P, Casadio R. I-Mutant2.0: predicting stability changes upon mutation from the protein sequence or structure. *Nucleic acids research* 2005; **33**(Web Server issue): W306-310.
34. Shihab HA, Gough J, Cooper DN, Stenson PD, Barker GLA, Edwards KJ, Day INM, Gaunt TR. Predicting the functional, molecular, and phenotypic consequences of amino acid substitutions using hidden Markov models. *Human mutation* 2013; **34**(1): 57-65.
35. Pejaver V, Byrne AB, Feng BL, Pagel KA, Mooney SD, Karchin R, O'Donnell-Luria A, Harrison SM, Tavtigian SV, Greenblatt MS, Biesecker LG, Radivojac P, Brenner SE, ClinGen Sequence Variant Interpretation Working Group. Calibration of computational tools for missense variant pathogenicity classification and ClinGen recommendations for PP3/BP4 criteria. *American journal of human genetics* 2022; **109**(12): 2163-2177.
36. Preston CG, Wright MW, Madhav Rao R, Harrison SM, Goldstein JL, Luo X, Wand H, Wulf B, Cheung G, Mark E Mandell ME, Tong H, Cheng S, Iacocca MA, Pineda AL, Popejoy AB, Dalton K, Zhen J, Dwight SS, Babb L, DiStefano M, O'Daniel JM, Lee K, Riggs ER, Zastrow DB, Mester JL, Ritter DI, Patel RY, Subramanian SL, Milosavljevic A, Berg JS, Rehm HL, Plon SE, Cherry JM, Bustamante CD, Costa HA, Clinical Genome Resource (ClinGen). ClinGen variant curation interface: a variant classification platform for the application of evidence criteria from ACMG/AMP guidelines. *Genome medicine* 2022; **14**(1): 6.
37. Tavtigian SV, Greenblatt MS, Harrison SM, Nussbaum RL, Prabhu SA, Boucher KM, Biesecker LG, ClinGen Sequence Variant Interpretation Working Group (ClinGen SVI). Modeling the ACMG/AMP variant classification guidelines as a Bayesian classification framework. *Genetics in medicine* 2018; **20**(9): 1054-1060.
38. Xiang S, Tong L. Crystal structures of human and *Staphylococcus aureus* pyruvate carboxylase and molecular insights into the carboxyltransfer reaction. *Nature structural & molecular biology* 2008; **15**(3): 295-302.
39. Kondo S, Nakajima Y, Sugio S, Sueda S, Islam MN, Kondo H. Structure of the biotin carboxylase domain of pyruvate carboxylase from *Bacillus thermodenitrificans*. *Acta crystallographica* 2007; **63**(Pt 8): 885-890.
40. Mochalkin I, Miller JR, Evdokimov A, Lightle S, Yan C, Stover CK, Waldrop GL. Structural evidence for substrate-induced synergism and half-sites reactivity in biotin carboxylase. *Protein science* 2008; **17**(10): 1706-1718.
41. Tsygankova P, Bychkov I, Minzhenkova M, Pechatnikova N, Bessonova L, Buyanova G, Naumchik I, Beskorovainiy N, Tabakov V, Itkis Y, Shilova N, Zakharova E. Expanding the genetic spectrum of the pyruvate carboxylase deficiency with novel missense, deep intronic and structural variants. *Molecular genetics and metabolism reports* 2022; **32**: 100889.
42. Babanejad M, Beheshtian M, Jamshidi F, M Mohseni M, Booth KT, Kahrizi K, Najmabadi H. Genetic etiology of hearing loss in Iran. *Human genetics* 2022; **141**(3-4): 623-631.
43. Cheraghi, S, Moghbelinejad S, Najmabadi N, Kimia Kahrizi, R Najafipour. The PTRHD1 Mutation in Intellectual Disability. *Archives of Iranian medicine* 2021; **24**(10): 747-751.
44. Tavasoli B, Safa M, Dorgalaleh A, Ghasemi JB, Makhouri FM, Rezvani MR, Ahmadi A, Tabibian S, Jazebi M, Baghaipour MR, Zaker F. Molecular and clinical profile of congenital fibrinogen disorders in Iran, identification of two novel mutations. *International journal of laboratory hematology* 2020; **42**(5): 619-627.
45. Bayat R, Koohmanae S, Nejat M, Kharaee F, Shahrokhi M, Hassanzadeh Rad A, Chakoosari SN, Dalili S, Hoseini Nouri SA. A case of pyruvate carboxylase deficiency with longer survival and normal laboratory findings. *Acta medica iranica* 2021; **59**(10): 4.
46. Ostergaard E, Duno M, Møller LB, Kalkanoglu-Sivri HS, Dursun A, Aliefendioglu D, Leth H, Dahl M, Christensen E, Wibrand F. Novel mutations in the PC gene in patients with type B pyruvate carboxylase deficiency. *JIMD reports* 2013; **9**: 1-5.
47. Breen C, White FJ, Scott CAB, Heptinstall L, Walter JH, Jones SA, Morris AAM. Unsuccessful treatment of severe pyruvate carboxylase deficiency with triheptanoin. *European journal of pediatrics* 2014; **173**(3): 361-6.
48. Hauser K, Negron C, Albanese SK, Ray S, Steinbrecher T, Abel R, Chodera JD, Wang L. Predicting resistance of clinical Abl mutations to targeted kinase inhibitors using alchemical free-energy calculations. *Communications biology* 2018; **1**: 70.
49. Fowler PW, Cole K, Gordon NC, Kearns AM, Llewelyn MJ, Peto TEA, Crook DW, Walker AS. Robust prediction of resistance to trimethoprim in *Staphylococcus aureus*. *Cell chemical biology* 2018; **25**(3): 339-349 e4.
50. Gapsys V, Michielssens S, Seeliger D, de Groot BL. Accurate and rigorous prediction of the changes in protein free energies in a large-scale mutation scan. *Angewandte chemie* 2016; **55**(26): 7364-7368.
51. Dietrich J, Lovell S, Veatch OJ, Butler MG. Phip gene variants with protein modeling, interactions, and clinical phenotypes. *American journal of medical genetics. Part A* 2022; **188**(2): 579-589.
52. Wang Y, Ma C, Jiang C, Zhang Y, Wu D. A novel IRF6 variant detected in a family with nonsyndromic cleft lip and palate by whole exome sequencing. *The Journal of craniofacial surgery* 2021; **32**(1): 265-269.